A SMART 6-DOF LOAD CELL DEVELOPMENT

S.M. Declercq, D.R. Lazor, and D.L. Brown

Structural Dynamics Research Laboratory
University of Cincinnati, P.O. Box 210072
Cincinnati, Ohio 45221-0072 USA

ABSTRACT

A smart 6-DOF load cell is developed which uses an array of ICP® strain gages with piezo-electric sensing elements. Since the strain gage transducers have multiple-pin connectors, Transducer Electronic Data Sheets (TEDS) can be used to identify each sensing element, thereby simplifying the cabling and eliminating channel identification errors. The TEDS of each strain gage also stores a single weighting value and a 6-element calibration factor. The weighting value is either 0 or 1, indicating the operational status of the sensor. The 6-element calibration factor converts the output of the sensor to its contribution to the 6-DOF force estimate. The result is a fault-tolerant smart 6-DOF load cell.

The load cell has been developed primarily for measuring 6-DOF impedance functions. Two case histories are presented to verify the load cell. The first is estimating rigid body inertia properties of a laboratory test structure. The second is the development of an impedance model of a standard laboratory test structure.

NOMENCLATURE

6-DOF = 6-degree-of-freedom
$[.]^+$ = pseudo-inverse of [.]
$\underline{q}$ = vector of rigid body translation accelerations
ADC = Analog to Digital Converter
$\underline{F}_p$ = vector of 6-DOF input forces at point p
FRF = frequency response function
$[G_{F_pF_p}]$ = auto spectral matrix of 6-DOF forces at point p
$[G_{X_{SG}F_p}]$ = cross spectral matrix between strain gage outputs and 6-DOF forces at point p
H_1 = H_1 FRF estimate $[G_{X_{SG}F_P}]\,[G_{F_PF_P}]^{-1}$
$[H_{LC}]$ = FRF matrix between load cell outputs and 6-DOF forces at point p; pseudo-inverse of load cell calibration matrix
[IM] = inertia matrix of rigid body mass
$\underline{K}_p$ = vector of rigid body modal participation factors; vector of 6 accelerations at point p
Nref = number of calibration mass tri-axial accelerometers
N_{SG} = number of strain gages in load cell
TEDS = Transducer Electronic Data Sheet
[W] = weighting matrix applied to exclude translation accelerations in calibration
$\underline{X}_{SG}$ = vector of strain gage responses
$[\psi]$ = rigid body transformation matrix

1. INTRODUCTION

In the historical development of multi-axis transducers, the mechanical structure, integrated sensing elements, and signal conditioning have been designed to isolate each axis of the transducer with minimal cross talk between the various axes. This required an elaborate mechanical design and manufacturing process. This type of design is not fault-tolerant, since a single component failure in the transducer would fail the transducer. In recent years, a revolution in technology has resulted in major advancements in signal conditioning, networking, and computing, due to developments in the consumer marketplace [1]. These advancements make it possible to develop a multi-sensor arrayed transducer with redundant sensing elements. Many more sensing elements are built into the transducer than the transducer has effective outputs (in the case of the 6-DOF load cell, the number of effective outputs is 6). Each sensing element is sensitive to multiple inputs, and a transformation matrix is used to generate the desired multi-axis transducer outputs. If one or more of the sensing elements fail, the desired outputs can still be generated from the remaining elements with a somewhat reduced dynamic range. This makes this type of transducer very fault-tolerant.

One of the technologies making this possible is the development of inexpensive 24-bit ADCs, which have been developed for the digital audio and video marketplace. These ADCs are inexpensive, have wide dynamic range (effectively 20-22 bits), and do not require additional signal processing other than what is currently built into ICP sensors. The multiple outputs of the arrayed transducer can be sampled with an inexpensive multi-channel data acquisition system using these new ADCs. The cost of the additional data acquisition channels is considerably less than the signal conditioning and ADCs of the previous generation of acquisition systems. With the wide dynamic range of the acquisition channels and the

redundant sensing elements, the arrayed transducer can provide fault-tolerant performance. Currently the arrayed transducers have analog outputs that are sampled with a conventional multi-channel data acquisition system. In the future, the acquisition of the sensing element data and the computation of the 6-DOF outputs will be integrated into the transducer or into a dedicated processor.

For the current 6-DOF load cell with analog outputs, it is very important for the data acquisition system to identify each sensing element. Therefore, each sensing element has an integrated Transducer Electronic Data Sheet (TEDS). The TEDS is used to identify the sensing element and to store a 1-bit weighting value of 0 or 1, indicating the operational status of the sensor. A value of 1 instructs the data analysis program to use that sensing element to generate the 6-DOF outputs of the load cell. A special TEDS template is currently being developed which will allow the storage of the sensitivity of each sensor to the six components of force acting on the 6-DOF load cell. All calibration information for the multi-axis sensing is then stored in the transducer. For the 6-DOF load cell, 6 sensitivity values will be stored in the TEDS of each sensing element.

In this paper, a newly developed smart 6-DOF load cell is evaluated. The evaluation includes calibration of the load cell, and verification of the load cell with rigid body inertia property estimation and impedance modeling applications. The sensors of the load cell are ICP strain gages that indirectly measure the dynamic force levels applied through the load cell. At least 6 strain gages are required to compute the 6-DOF forces. A larger number of sensors are used for fault-tolerance, allowing for individual sensor failure and a least-squares solution for the calibration matrix.

The 6-DOF load cell is calibrated using a rigid body calibration mass instrumented with accelerometers at known positions. The use of rigid body inertia properties and Newton's 2nd Law of motion, F=ma, yields a calibration matrix that transforms the strain gage responses to the 6-DOF forces (3 translation forces and 3 moments) applied through the load cell. For N_{SG} number of strain gages, the $6xN_{SG}$ calibration matrix is stored by columns in the TEDS of each sensor, and used to estimate the 6-DOF forces when the load cell is used in other applications.

Two applications of the calibrated 6-DOF load cell are presented in this paper. The first application uses the load cell to estimate inertia properties of a rigid body mass. The results are compared to the known rigid body inertia properties. Agreement is within approximately 1-10% error, depending on the accuracy of the mass modeling and the accelerometer positions. The second application of the load cell is impedance modeling of an H-frame structure. Impedance functions modeled using the 6-DOF load cell agree well with those modeled and physically measured using the indirect method.

2. ICP STRAIN GAGE 6-DOF LOAD CELL

The 6-DOF load cell evaluated in this paper consists of a circular aluminum ring of outer diameter 11.4cm, inner diameter 7.6cm, and thickness 1.3cm, as shown in Figure 1. Four spokes of length 2.5cm and cross-section 1cm connect the center of the ring to the edges of the ring. The spokes are fairly stiff and were designed to exhibit sufficient strain under dynamic loading to be detected by the strain gages. The current ICP strain gages are very sensitive, with values of approximately ½ V per micro-strain, and are electrically attenuated by a factor of 100. The attenuation can be removed and the strain gage sensing element made even stiffer (and hence more sensitive) than it currently is if a stiffer load cell design is required.

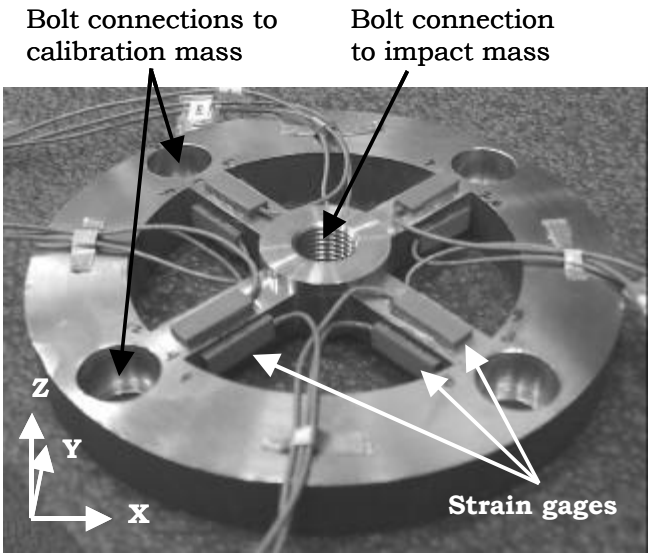

Figure 1: *ICP strain gage placement on 6-DOF load cell.*

12 ICP strain gages are super-glued to the flat surfaces of the four spokes, as shown in Figure 1. Using 12 strain gages results in a fault-tolerant load cell, with an over-determination factor of 2 for the least squares calibration solution. The current load cell design has 4 strain gages in the x-y plane, 2 in the x-y plane, 4 in the x-z plane, and 4 in the y-z plane. There is sufficient redundancy in this configuration to allow for sensor failure and still have an operational load cell. Of course, ideally a finite element model of the load cell structure would be built to determine the optimal number and placement of the strain gages for maximum strain output and fault-tolerance.

The forces are applied to the load cell through the center bolt of the load cell and cause strains in the spokes, which are measured by the strain gages. The applied forces are transmitted to the calibration mass

through four bolts attaching the load cell to the calibration mass. By relating the load cell strains to the forces estimated using rigid body inertia properties, rigid body motion, and the law F=ma, the load cell can be calibrated to indirectly measure the 6-DOF forces.

The ICP strain gage 6-DOF load cell combines the wide dynamic range of piezo-electric crystals with the measurement practicality of strain gages.

2.1 Comparison with stacked-crystal 6-DOF load cell

Previously, a 6-DOF load cell with stacked piezo-electric crystals was developed [2-6] and used to estimate the rigid body inertia properties of various structures, including the X-38 vehicle. The main problem encountered with the stacked-crystal load cell was its sensitivity to preload.

The stacked-crystal load cell has 4 ring-shaped crystals segmented into 2 compression pairs and 2 shear pairs, resulting in a total of 8 crystal outputs. The piezo-electric crystal surfaces must be very flat in order to consistently make full contact with the other crystals. To ensure the crystal surfaces were mated properly, a large preload had to be applied to the load cell prior to calibration and use. Modifying the preload on the crystals affects the crystal surface contact area and output of the load cell, so the applied preload had to be much larger than any effective preload applied during an application test of the load cell.

In the case of the X-38 test, large moments applied to the stacked-crystal load cell via the test fixture increased the effective preload on the crystals and possibly altered the contact surface mating and output of the load cell [6]. The ICP strain gage load cell does not use the stacked-crystal design, and is much less sensitive to preloading. The piezo-electric crystals of the ICP strain gages are not used in compression, and so preload does not need to be applied.

The calibration matrix for the stacked 8-crystal load cell is 6x8 in size. A minimum of 6 outputs is needed to resolve the 6-DOF forces, so it would appear that a crystal sensing element could fail and the load cell would still be operational. This is true if the failed sensing element is one of the compression crystals. However, if one of the shear crystals fails, the information along that axis cannot be resolved. Therefore, the stacked 8-crystal load cell does not have overall fault-tolerance capabilities.

2.2 Comparison with static strain gage load cell

Other strain gage 6-DOF load cells exist, using static strain gages. Typically, these static strain gage load cells are not standard off-the-shelf products, but are designed and built in-house for specific applications. The advantages of the ICP strain gage load cell include dynamic force sensitivity, or improved dynamic range, and increased fault-tolerance.

The ICP strain gage load cell uses piezo-electric sensing elements, so the load cell does not estimate static forces, only dynamic forces. The dynamic force levels are typically much lower in level than the static forces, so an ICP strain gage can be made more sensitive to detect those levels. The current ICP strain gages are very sensitive (on the order of ½ V per micro-strain) and are attenuated electronically by a factor of 100. The sensitivity can be controlled electronically, or the sensor can be made even more sensitive by increasing the stiffness of the beam in the sensing element. The increased sensitivity to dynamic forces results in a wider dynamic range.

The static strain gage load cells have strain gages placed so that they are sensitive to particular forces and moments. There is usually little or no built-in redundancy. The ICP strain gage load cell has built-in redundancy. Therefore, if a sensor of the load cell fails, the load cell will still be operational.

Static strain gages can be applied to a non-flat surface. The current ICP strain gages have a flat metal casing, and therefore require a flat surface to adhere to. Since the load cell structure developed is somewhat arbitrary, it is not difficult to machine flat load cell surfaces for the strain gages. However, the metal casing design can be modified to adhere to non-flat surfaces if needed.

In conclusion, it is hoped that the ICP strain gage 6-DOF load cell will be an improvement over previous 6-DOF load cells in the areas of preload sensitivity, measurement of dynamic force levels, and fault-tolerance.

3. CALIBRATION OF THE 6-DOF LOAD CELL

The indirect measurement of the 6-DOF forces applied through the load cell is based on Newton's 2nd Law, F=ma, and the use of an instrumented rigid body mass with known inertia properties. The theory for the 6-DOF load cell calibration is reviewed in Section 3.1. Section 3.2 outlines the calibration procedure, and Section 3.3 presents the load cell calibration results.

3.1 6-DOF load cell calibration theory

The goal of the load cell calibration is to relate the strain gage responses of the load cell to the 6-DOF forces at a point p located at the base of the load cell, as shown in Figure 2.

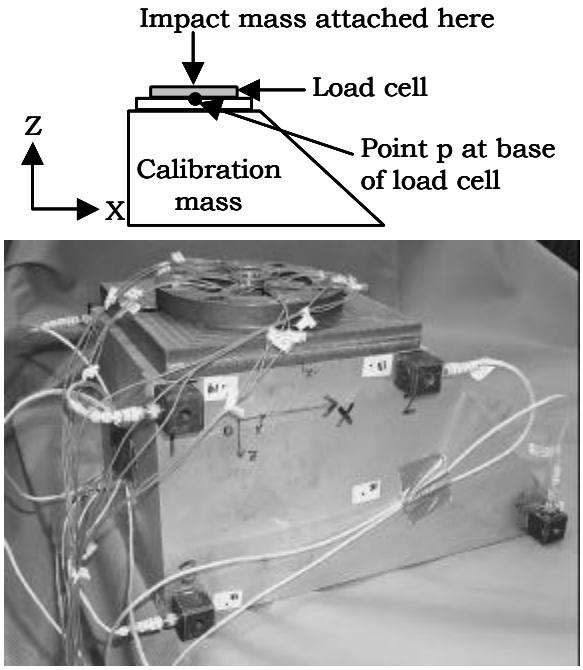

Figure 2: *Calibration point p at base of 6--DOF load.*

The relationship between the outputs of the load cell, $\underline{X}_{SG}$, and the 6-DOF forces at point p, $\underline{F}_p$, is expressed in the frequency domain as

$$\underline{X}_{SG} = [H_{LC}]\underline{F}_p \quad , \tag{1}$$

where $[H_{LC}]$ is the frequency response function (FRF) matrix between $\underline{X}_{SG}$ and $\underline{F}_p$. Once $[H_{LC}]$ is known, the load cell can be used in various applications to estimate the 6-DOF forces at point p. This is done by measuring the strain gage responses and solving equation (1) for the forces

$$\underline{F}_p = [H_{LC}]^{+}\underline{X}_{SG} \quad . \tag{2}$$

At least 6 strain gages are needed to solve equation (2), but a larger number of sensors allows for both fault-tolerance and a pseudo-inverse least-squares solution.

In order to compute $[H_{LC}]$, the vector $\underline{F}_p$ must first be calculated. This is done by using a rigid body calibration mass of known inertia properties, instrumented with accelerometers at known positions. The load cell is attached to the calibration mass and an impact mass is attached to the other side of the load cell, as shown in Figure 3. The entire calibration fixture is suspended with soft cables to simulate a free-free boundary condition.

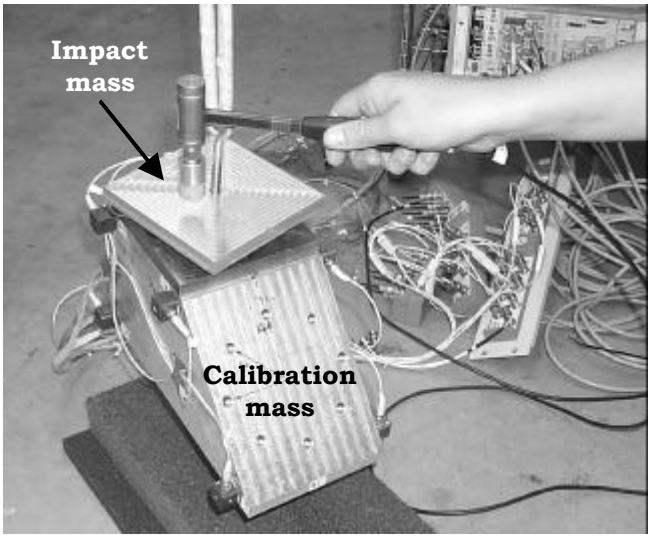

Figure 3: *Load cell with impact mass and rigid body calibration mass.*

Impacts are applied to the impact mass. All forces exciting the calibration mass must travel through the load cell. The known or measured quantities are the strain gage responses due to the applied inputs, the inertia properties of the rigid body mass, and the translation acceleration responses of the calibration mass. The translation accelerations and inertia properties of the calibration mass are used to compute $\underline{F}_p$. $\underline{F}_p$ and the strain gage responses $\underline{X}_{SG}$ are used to compute $[H_{LC}]$.

The F=ma law can be expressed in terms of the 6-DOF forces, the inertia matrix, and the 6-DOF accelerations, at a point p on the rigid body,

$$\begin{bmatrix} F_x \\ F_y \\ F_z \\ M_x \\ M_y \\ M_z \end{bmatrix}_p = \begin{bmatrix} m & 0 & 0 & 0 & mz_{cg} & -my_{cg} \\ 0 & m & 0 & -mz_{cg} & 0 & mx_{cg} \\ 0 & 0 & m & my_{cg} & -mx_{cg} & 0 \\ 1 & 0 & 0 & I_{xx} & -I_{xy} & -I_{xz} \\ 0 & 1 & 0 & -I_{xy} & I_{yy} & -I_{yz} \\ 0 & 0 & 1 & -I_{xz} & -I_{yz} & I_{zz} \end{bmatrix} \begin{bmatrix} \ddot{x} \\ \ddot{y} \\ \ddot{z} \\ \ddot{q}_x \\ \ddot{q}_y \\ \ddot{q}_z \end{bmatrix}_p \tag{3}$$

where F_x, F_y and F_z are the three translation forces at point p, and M_x, M_y, and M_z are the three moments at point p.

By measuring the translation accelerations from the calibration mass, the three translation and three rotation accelerations at any point p on the rigid body can be computed [7]. The translation $\underline{q}$ of any point i on a rigid body can be described as a superposition of the rigid body modes,

$$\underline{q}_i = [\Psi_i]\underline{K}_p \quad , \tag{4}$$

where $[\psi_i]$ is the rigid body transformation matrix for point i and $\underline{K}_p$ is the vector of six modal participation factors. If the rigid body modes are scaled to unity displacement at point p, $\underline{K}_p$ is equal to the translation and rotation accelerations at point p,

$$\begin{bmatrix} \ddot{x}_i \\ \ddot{y}_i \\ \ddot{z}_i \end{bmatrix} = \begin{bmatrix} 1 & 0 & 0 & 0 & z_i & -y_i \\ 0 & 1 & 0 & -z_i & 0 & x_i \\ 0 & 0 & 1 & y_i & -x_i & 0 \end{bmatrix} \begin{bmatrix} \ddot{x} \\ \ddot{y} \\ \ddot{z} \\ \ddot{q}_x \\ \ddot{q}_y \\ \ddot{q}_z \end{bmatrix}_p \quad , \quad (5)$$

where x_i, y_i, and z_i indicate the position of point i in a coordinate system with origin point p. To solve for the six accelerations at point p, at least six independent pieces of information are needed. By including additional measurement points, the system can be over-determined and a least-squares solution obtained. Equation (4) is expanded as

$$\underline{q} = \begin{bmatrix} \underline{q}_1 \\ \underline{q}_2 \\ \vdots \\ \underline{q}_{Nref} \end{bmatrix} = \begin{bmatrix} [\Psi_1] \\ [\Psi_2] \\ \vdots \\ [\Psi_{Nref}] \end{bmatrix} \underline{K}_p \quad , \quad (6)$$

where *Nref* is the number of tri-axial accelerometers on the calibration mass.

A diagonal weighting matrix [W] can be used to select the accelerations to be included in the solution. Any accelerometer that has failed, or otherwise produces erroneous data, can be removed from the calibration process by zeroing out its corresponding element in [W]. Pre-multiplying both sides of equation (6) by the weighting matrix [W] and solving for $\underline{K}_p$ using a least-squares pseudo-inverse procedure results in

$$\underline{K}_p = ([W][\Psi])^+ [W]\underline{q} \quad . \quad (7)$$

Equation (7) estimates the translation and rotation accelerations at a point p on the rigid body, based on the translation accelerations of the calibration mass. The resulting 6-dOF forces at point p are estimated from the motion of the calibration mass using F=ma. Substituting $\underline{K}_p$ from equation (7) into equation (3) results in

$$\underline{F}_p = [IM]\underline{K}_p = [IM]([W][\Psi])^+ [W]\underline{q} \quad , \quad (8)$$

where $\underline{F}_p$ is the vector of 6-DOF forces at point p and [IM] is the inertia matrix expressed in equation (3).

Equation (8) relates the 6-DOF forces at point p to the *Nref* tri-axial translation accelerations from the calibration mass. The relationship between the load cell outputs and the 6-DOF forces was given in equation (1) as

$$\underline{X}_{SG} = [H_{LC}]\underline{F}_p \quad . \quad (1)$$

The matrix $[H_{LC}]$ is calculated using an H_1 FRF estimate

$$[H_{LC}] = [G_{X_{SG}Fp}][G_{FpFp}]^{-1} \quad , \quad (9)$$

where $[G_{X_{SG}F_p}]$ is the cross spectral matrix between the load cell outputs and the 6-DOF forces at point p, and $[G_{F_pF_p}]$ is the auto spectral matrix of the 6-DOF forces at point p. Averaging in the FRF estimate is done by impacting at different locations and directions on the impact mass to excite all degrees of freedom of the calibration mass.

The inverse of the $[H_{LC}]$ matrix is of size $6xN_{SG}$, where N_{SG} is the number of strain gages, and is the calibration matrix of the load cell. Post-multiplying this calibration matrix by the strain gage responses yields the 6-DOF forces.

3.2 6-DOF load cell calibration procedure

In the calibration procedure, impacts are applied to the impact mass in various locations and directions in an attempt to excite all possible motion of the calibration mass. In addition, the load cell is tested in multiple configurations on the calibration mass to better excite the calibration mass. Measurements of the direct forces applied to the impact mass via an instrumented impact hammer are not used in the calibration process.

To provide averaging for the H_1 FRF estimation procedure, 50 impacts were applied to the impact mass in various locations and directions for each of the 6 configurations tested, and the strain gage and accelerometer responses were measured. This was repeated for each of the 6 configurations tested. Figure 4 shows the 6 different configurations of the load cell on the calibration mass.

A rigid body check is performed on the data to determine if any of the accelerometers have failed, have high noise floors, possibly have position errors, or otherwise produce non-consistent data [5]. A total of 6 independent accelerations are needed for an exact solution. 8 tri-axial accelerometers were used so there is an over-determination factor of 4, allowing for removal of outlying signals and a least-squares solution to the problem.

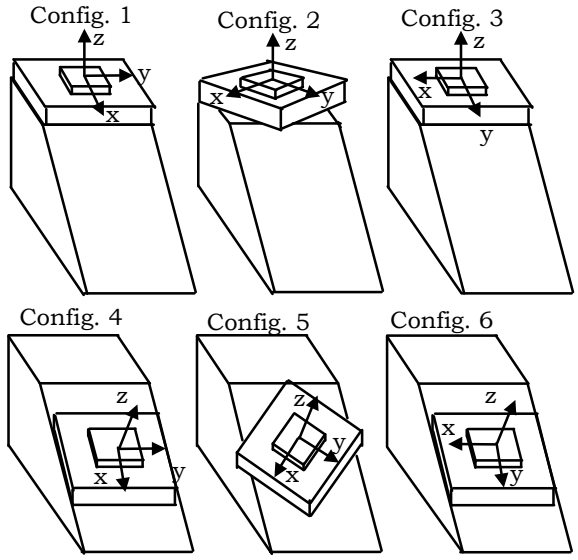

Figure 4: *6 test configurations of the load cell and rigid body mass.*

An H_1 FRF estimate, using the strain gage responses as outputs and the 6-DOF forces computed from the rigid body mass accelerations as inputs, is performed to compute a complex, frequency-dependent N_{SG}x6 size $[H_{LC}]$ matrix. The H_1 FRF estimate is performed on all 6 configurations simultaneously.

The curves of the frequency-dependent $[H_{LC}]$ matrix are fairly flat in the frequency range of interest, thus a real or complex frequency-independent matrix can be computed. The full frequency-dependent matrix could be used if the curves were not flat, requiring more storage space.

The pseudo-inverse of the N_{SG}x6 size $[H_{LC}]$ matrix is the calibration matrix of the load cell. The $[H_{LC}]$ matrix must be well-conditioned to perform a pseudo-inverse, since some amount of measurement noise is always present. The 6xN_{SG} matrix is then stored by columns in the TEDS of each strain gage, and multiplied by the N_{SG}x1 strain gage response vector in various applications. The result is the 6-DOF force vector.

If a strain gage of the load cell fails, the load cell can still be operational. In that case, the weighting value in the TEDS of that sensor is set to 0. The row in the N_{SG}x6 size $[H_{LC}]$ matrix corresponding to the failed sensor is removed and the pseudo-inverse of $[H_{LC}]$ recomputed. The resulting matrix of size 6x(N_{SG}-1) is stored (by columns) in the TEDS of the functional strain gages.

3.3 6-DOF load cell calibration results

The calibration data were acquired in the 0-256 Hz frequency range with a ½ Hz frequency resolution. The impact mass, load cell, and rigid body calibration mass have no deformation modes in this frequency range. An exponential window with a 1% end damping value was applied to the time domain data before the FFT to reduce leakage.

Figure 5 shows sample force and moment calibration curves. The curves are relatively flat in the 50-200 Hz frequency range. An average of the curve values was selected for the 50-200 Hz frequency range.

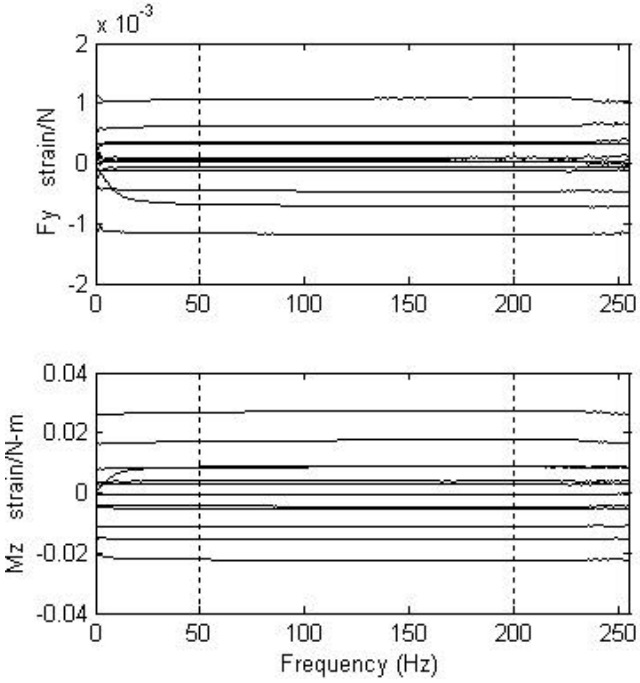

Figure 5: *Sample force and moment calibration curves of the ICP strain gage 6-DOF load cell.*

The resulting $[H_{LC}]$ matrix has a condition number below 60. This value is acceptable for the pseudo-inversion solution process.

4. APPLICATION 1: ESTIMATION OF RIGID BODY INERTIA PROPERTIES

The calibrated load cell is used to estimate the inertia properties of a rigid body mass shown in Figure 6. The rigid body mass is a steel block of dimensions 15.2cm x 15.2cm x 33.2cm. The inertia properties of the rigid body mass were computed using AutoCAD to compare with the load cell estimates.

8 tri-axial accelerometers were attached to the 8 corners of the mass to measure the translation motion due to the applied inputs. The load cell was attached to the rigid body mass in the same manner as the calibration mass. The impact mass was then bolted to the top of the load cell. 50 impacts were applied to the impact plate in various locations and directions, and the strain gage and accelerometer responses were

measured. Data were acquired in the 0-256 Hz frequency range, with a frequency resolution of ¼ Hz.

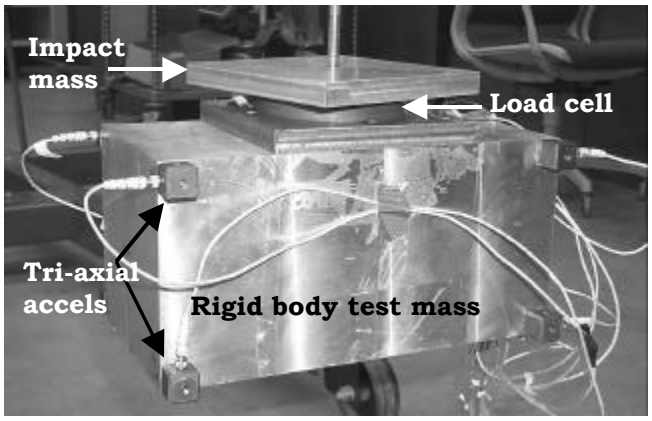

Figure 6: *Rigid body mass used for inertia estimation.*

The load cell calibration matrix was applied to the strain gage responses to compute the 6-DOF force estimate at the base of the load cell. These 6-DOF forces were then used with the accelerometer responses to estimate the inertia properties of the rigid body mass. Figure 7 shows the estimated mass, center of gravity positions, and inertia values, as a function of frequency. The estimates are very flat in the 50-200 Hz frequency range, allowing an average of the values to be computed in this range.

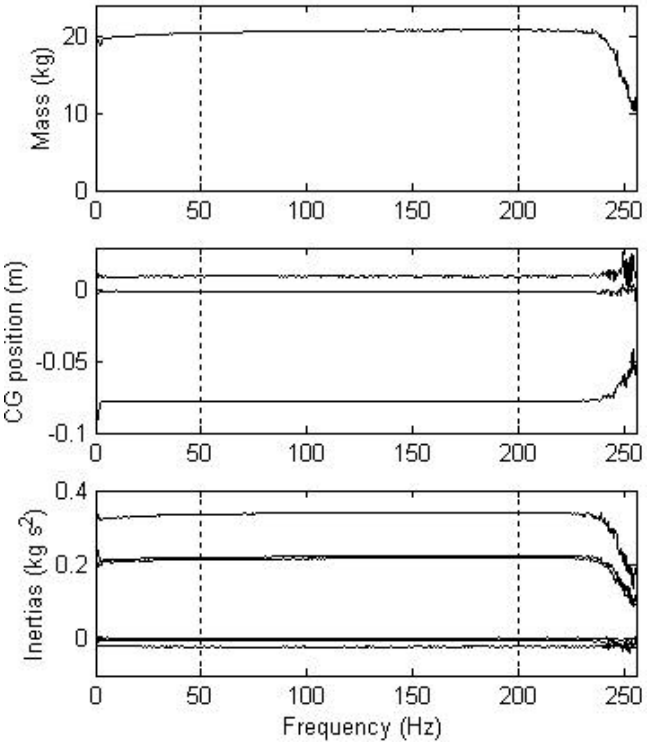

Figure 7: *Sample estimated inertia property values.*

Table 1 presents the estimated and actual inertia properties of the rigid body mass. For all non-zero values, the estimates are within approximately 10% error. For the values presented in Table 1, the accelerometer positions are accurate within 4-11%. With more accurate position values, the inertia property estimate errors can be reduced to 1-5%. These results verify the validity of the ICP strain gage load cell in estimation of rigid body inertia property applications.

	Actual	Estimated	Error
Mass (kg)	21.395	20.665	5.8 %
Xcg (m)	3.013E-4	9.8551E-3	---
Ycg (m)	1.725E-5	-8.0125E-4	---
Zcg (m)	-0.08075	-0.07785	3.6 %
Ixx (kg s²)	0.24011	0.22169	7.7 %
Ixy (kg s²)	5.0E-5	1.5069E-3	---
Ixz (kg s²)	7.496E-4	-2.2449E-2	---
Iyy (kg s²)	0.38056	0.338695	11.0 %
Iyz (kg s²)	5.0E-5	-4.3728E-3	---
Izz (kg s²)	0.22665	0.215889	4.7 %

Table 1: *Actual and estimated inertia properties.*

5. APPLICATION 2: IMPEDANCE MODELING OF H-FRAME STRUCTURE

Impedance modeling requires accurate impedance measurements at the component connection points. A 6-DOF impedance FRF matrix can be determined using the indirect method [8] by performing a multiple-reference impact test and resolving the inputs and outputs to a single point on the rigid body. The indirect method requires known input and output locations and directions, and is thus sensitive to any impact location and direction errors. As an alternative to the indirect method, the calibrated 6-DOF load cell can be used to measure the 6-DOF input forces at the connection point, and thus obtain more accurate impedance functions [8].

The baseline test structure used for the impedance modeling is an H-frame, shown in Figure 8, constructed of steel box tubing with aluminum endplates. A steel plate connected to one of the aluminum endplates served as a sub-structure for the impedance modeling.

The total mass of the baseline H-frame is 110 kg. The H-frame was designed to be relatively uncoupled in the some directions, with a high degree of coupling in other directions. The first deformation mode of the aluminum endplates is at 918 Hz, so each endplate acts as a rigid body at lower frequencies. In the rigid body frequency range, translation measurements made on an endplate can be transformed to 6-DOF impedance functions at the sub-structure connection point on the endplate.

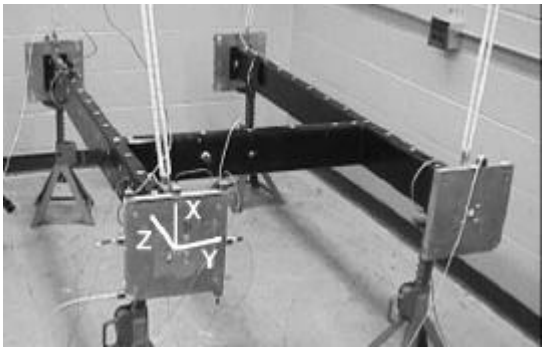

Figure 8: *Baseline H-frame with aluminum endplates.*

A single steel plate of mass 15.2 kg, shown in Figure 9, was connected to one of the endplates as a sub-structure for use with the impedance models. The FRFs for the added steel plate were analytically computed from the mass inertia matrix. The plate sub-structure was modeled in AutoCAD. The inertia matrix was obtained from the mass of the steel plate, its center of gravity positions, and its inertia properties.

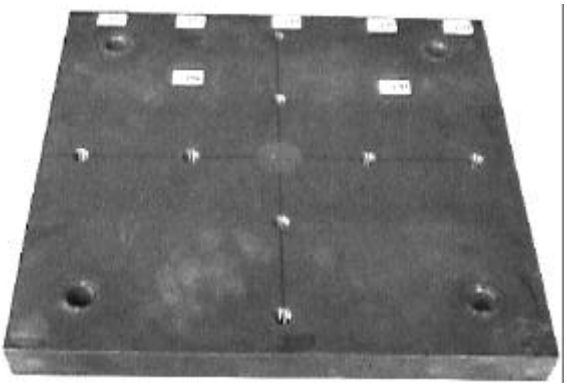

Figure 9: *Single steel plate used as sub-structure.*

Three sets of impedance functions are presented for comparison purposes. The first set is modeled impedance functions, obtained with the 6-DOF load cell measurements made on the baseline H-frame, which were then analytically coupled to the sub-structure. The second set is modeled impedance functions using indirect 6-DOF measurements made on the baseline H-frame, analytically coupled to the sub-structure. The third set is measured impedance functions using indirect 6-DOF measurements made on the physically modified H-frame with the steel plate bolted to one of the aluminum endplates.

For the first set of impedance functions, the calibrated load cell was attached to the aluminum endplate of the baseline H-frame, as shown in Figure 10. An impact plate was attached to the other side of the load cell. Impacts were applied to the impact plate in various directions and locations to excite the H-frame. All forces applied to the H-frame pass through the load cell. The translation motion of the endplate was measured using 8 tri-axial accelerometers located at the 8 corners of the aluminum endplate. The translation accelerations were transformed to the 6-DOF accelerations at the center of the endplate, assuming rigid body motion. The 6-DOF forces were computed from the calibrated load cell and used in conjunction with the 6-DOF accelerations to obtain the 6-DOF FRFs for impedance modeling. The 6-DOF impedance functions of the baseline H-frame were then analytically connected to the steel plate using impedance modeling.

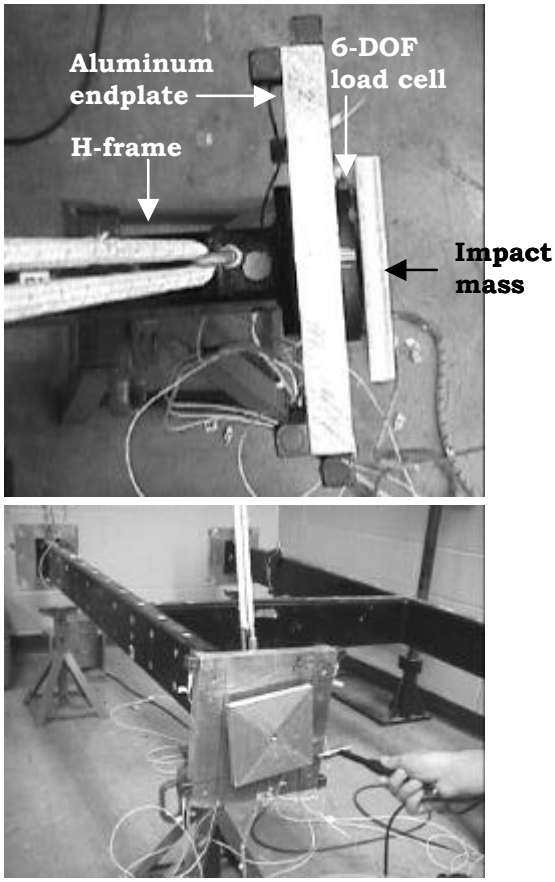

Figure 10: *Impedance measurements on baseline H-frame using calibrated 6-DOF load cell.*

For the second set of impedance functions, indirect 6-DOF measurements were made by impacting on the baseline H-frame aluminum endplate in 19 locations and directions, as shown in Figure 11, and measuring the FRFs between the N_i inputs and N_o translation accelerations from 8 tri-axial accelerometers located on the 8 plate corners. As long as the endplate behaves as a rigid body in the frequency range of interest, input and output transformation matrices can be formulated and used to transform the $N_o x N_i$ FRF matrix to a 6x6 FRF matrix at the center of the endplate [8]. This transformation requires the input

and output locations and directions. For the indirect method impedance modeling, the 6-DOF impedance functions measured on the baseline H-frame were analytically coupled to the sub-structure.

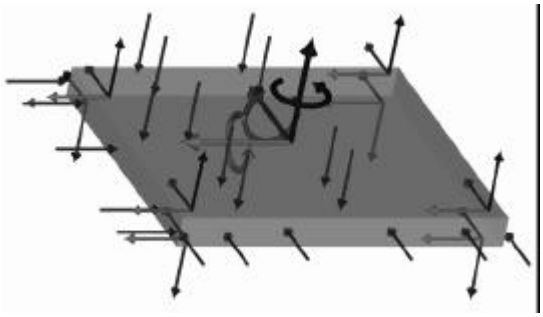

Figure 11: *Impedance measurements on baseline H-frame endplate using indirect method.*

The third set of impedance functions are measured, using the indirect method applied to the physically modified H-frame with the steel plate bolted to the end of one of the aluminum endplates, as shown in Figure 12.

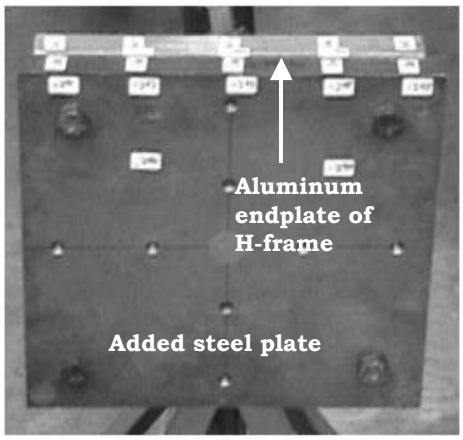

Figure 12: *Physically modified H-frame with steel plate added to aluminum endplate.*

The disadvantage of the indirect method compared to the load cell method is that the indirect method is very sensitive to any errors in input and output locations and directions. Since it is fairly simple to place and align the accelerometers, this difficulty refers mostly to the impact input.

The data for each of the three tests were acquired in the 0-800 Hz frequency range, with a frequency resolution of ½ Hz. 19 impacts were used in the two indirect methods, and 60 impacts for the load cell method. Figures 13 and 14 compare the driving point impedance model results with the data taken on the physically modified system.

For the x-axis and y-axis translation FRFs and the z-axis rotation FRF, Figure 13 shows good correlation between the modeled impedance functions (indirect method and 6-DOF load cell method applied to the baseline H-frame, with analytical coupling to steel plate) and the measured impedance functions (indirect method applied to physically modified H-frame with added steel plate). Some discrepancies occur at the higher frequencies. Modes from the baseline system that exist higher than the measured frequency range are lowered by the addition of the mass. It is not possible to model these effects using FRFs, since the mode contributions do not appear in the baseline data. The modes that are lowered into the frequency range of interest are measured on the physically modified system, hence the discrepancies at the higher frequencies.

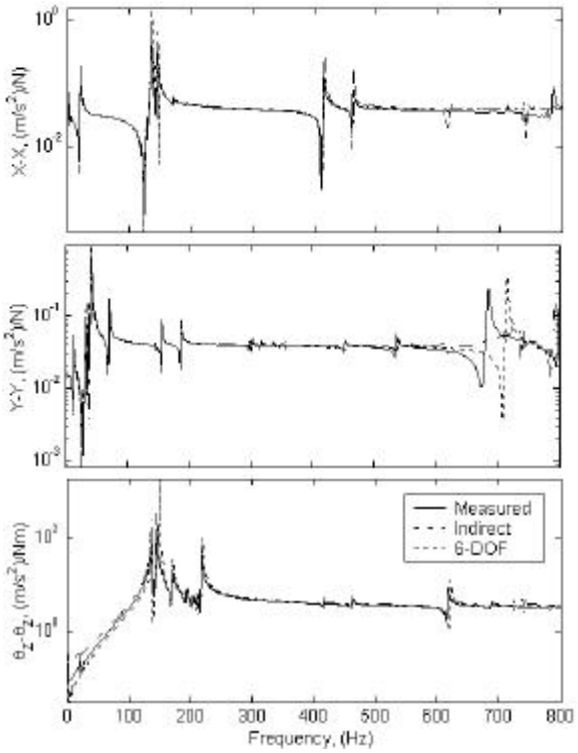

Figure 13: *Driving point impedance model and physical measurement results for x-axis and y-axis translations and z-axis rotation.*

Figure 14, however, shows large variations between the modeled and measured impedance functions for the z-axis translation FRF, and for the x-axis and y-axis rotation FRFs, which are directly affected by z-axis translation errors. These variations occur because it is very difficult to measure accurate z-axis translation accelerations, due to the high stiffness of the H-frame in the z-direction. Errors in the z-axis

translation accelerations cause errors in the 6-DOF accelerations computed at the connection point due to the indirect method computation. All three methods contain these errors. The two indirect methods have additional errors because the *z*-axis direction is very sensitive to impact location and direction errors.

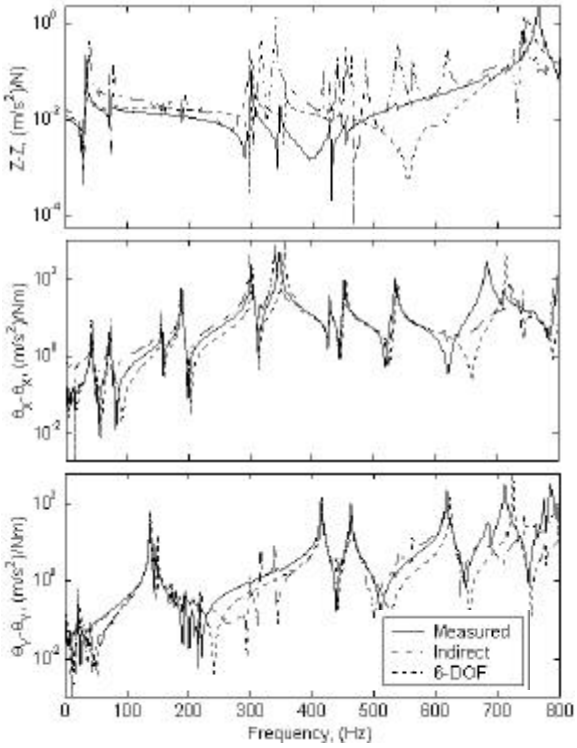

Figure 14: *Driving point impedance model and physical measurement results for z-axis translation and x-axis and y-axis rotations.*

6. CONCLUSIONS

A new 6-DOF load cell using ICP strain gages has been developed and evaluated in this paper. The load cell combines the wide dynamic range capabilities of piezo-electric crystals with the measurement practicality of strain gages.

Each strain gage of the load cell stores a 1-element weighting value and a 6-element calibration factor in its TEDS. Therefore, all calibration information for the load cell is stored in the load cell. Using a redundant number of sensors, with the option to remove failed sensors via the 1-element weighting value in the TEDS, results in a fault-tolerant load cell.

The 6-DOF load cell was calibrated and applied to inertia property estimation and impedance modeling. Inertia properties of a rectangular rigid body mass were estimated within approximately 10% error. The errors can be further reduced to 1-5% with more accurate accelerometer positions. Impedance functions were modeled using 6-DOF load cell measurements taken on an H-frame structure, analytically connected to a steel plate sub-structure. These impedance functions agreed well with modeled impedance functions using the indirect method on the H-frame analytically connected to the sub-structure, and with measured impedance functions using the indirect method on the physically modified H-frame.

7. ACKNOWLEDGEMENTS

The authors would like to thank PCB Piezotronics Inc. and The Modal Shop Inc. for the use of their equipment.

ICP is a registered trademark of PCB Piezotronics Inc.

8. REFERENCES

[1] Brown, D.L., Dumbacher, S., and D. Adams, *Impact of the Consumer Marketplace upon Structural Dynamics, Controls and Acoustics*, Proc. of the 19th International Modal Analysis Conference, Orlando, FL, 2001.

[2] Stebbins, M.A., *Calibration and Application of Multi-Axis Load Cells*, Masters Thesis, 1997, University of Cincinnati.

[3] Stebbins, M.A and D.L. Brown, *Rigid Body Intertia Property Estimation Using a Six-axis Load Cell*, Proc. of the 16th International Modal Analysis Conference, Santa Barbara, CA, 1998.

[4] Witter, M.C., Brown, D.L., and R.W. Bono, *Broadband 6 DOF Accelerometer Calibration Via Impact Excitation*, Proc. of the 16th International Modal Analysis Conference, Santa Barbara, CA, 1998.

[5] Witter, M.C., Blough, J.R., and D.L. Brown, *Measuring the 6 Degree of Freedom Driving Point Frequency Response Function Using a 6 DOF Impedance Head and its Validation*, Proc. of the 23rd International Seminar on Modal Analysis, Leuven, Belgium, September 1998.

[6] Witter, M.C., Brown, D.L., and M. Dillon, *A New Method for RBP Estimation – The Dynamic Inertia Method*, Society of Allied Weight Engineers, SAWE Paper No. 2461, 1999.

[7] Li, S., Brown, D.L., Seitz, A., and M. Lally, *The Development of Six-Axis Arrayed Transducer*, Proc. of the 12th International Modal Analysis Conference, 1994.

[8] Lazor, D.R. and D.L. Brown, *Impedance Modeling with Multiple Axis Load Cells*, Proc. of the 20th International Modal Analysis Conference, Los Angeles, CA, 2002.